

**NASA**

W-34  
397619

# MEMORANDUM

AN INVESTIGATION OF THE EFFECT OF A HIGHLY FAVORABLE  
PRESSURE GRADIENT ON BOUNDARY-LAYER TRANSITION  
AS CAUSED BY VARIOUS TYPES OF ROUGHNESSES  
ON A 10-FOOT-DIAMETER HEMISPHERE  
AT SUBSONIC SPEEDS

By John B. Peterson, Jr., and Elmer A. Horton

Langley Research Center  
Langley Field, Va.

**NATIONAL AERONAUTICS AND  
SPACE ADMINISTRATION**

WASHINGTON

April 1959



NATIONAL AERONAUTICS AND SPACE ADMINISTRATION

MEMORANDUM 2-8-59L

AN INVESTIGATION OF THE EFFECT OF A HIGHLY FAVORABLE  
PRESSURE GRADIENT ON BOUNDARY-LAYER TRANSITION  
AS CAUSED BY VARIOUS TYPES OF ROUGHNESSES  
ON A 10-FOOT-DIAMETER HEMISPHERE  
AT SUBSONIC SPEEDS

By John B. Peterson, Jr., and Elmer A. Horton

SUMMARY

Tests were made on a 10-foot-diameter hemispherical nose at Reynolds numbers up to  $10 \times 10^6$  and at a maximum Mach number of about 0.1 to determine the effects of a highly favorable pressure gradient on boundary-layer transition caused by roughness. Both two-dimensional and three-dimensional roughness particles were used, and the transition of the boundary layer was determined by hot-wire anemometers. The roughness Reynolds number for transition  $R_{k,t}$  caused by three-dimensional particles such as Carborundum grains, spherical particles, and rimmed craters was found. The results show that for particles immersed in the boundary layer,  $R_{k,t}$  is independent of the particle size or position on the hemispherical nose and depends mainly on the height-to-width ratio of the particle. The values of  $R_{k,t}$  found on the hemispherical nose compare closely with those previously found on a flat plate and on airfoils with roughness. For two-dimensional roughness, the ratio of roughness height to boundary-layer displacement thickness necessary to cause transition was found to increase appreciably as the roughness was moved forward on the nose. Also included in the investigation were studies of the spread of turbulence behind a single particle of roughness and the effect of holes such as pressure orifices.

INTRODUCTION

The nature of boundary-layer transition caused by surface roughness has long been of general interest in connection with drag estimation of airplanes, and with the advent of high altitude and high Mach number missiles new emphasis is added to the field by the dependence of the

aerodynamic heating problem on the character of the boundary layer over the blunted noses of such devices.

Previous investigations (refs. 1 to 6) of the effects of three-dimensional roughness particles on boundary-layer transition have shown that a critical roughness height for transition can be expressed in the form of a roughness Reynolds number based on roughness height, velocity, and viscosity conditions at the top of the roughness particle. This investigation was made to extend these results to the case of three-dimensional flow on a body having a large stabilizing pressure gradient and high Reynolds numbers.

Since there are no wind tunnels which can duplicate the Mach numbers and Reynolds numbers found on missile noses, tests must be made with very expensive rockets with highly polished noses if all in-flight conditions are to be duplicated. However, in an investigation of the effects of roughness, it is desirable to use roughness sizes which can be easily detected and measured and to be able to inspect the surface of the body after the test to determine if the surface has been contaminated with extraneous roughness particles. Therefore, consideration was given to the use of a body of large diameter in low-speed flow in order to allow the use of practical roughness sizes and still to retain the high Reynolds numbers that are of interest in high-speed work. It was thought that if the high Reynolds number of the flow was maintained, the results of a test at subsonic speeds would be generally applicable to the problem of roughness-induced transition at supersonic speeds inasmuch as reference 6 has shown that the critical roughness Reynolds number is independent of Mach number for the range of Mach numbers tested (up to a Mach number of 2) if the properties of the air at the top of the roughness are used. Also, the flow behind the detached shock of blunt-nosed bodies is subsonic near the stagnation point; therefore, the Mach number may not have a large influence on transition in these cases except for the effect of the large temperature gradient that may exist in the boundary layer. Consequently, a 10-foot-diameter body with a hemispherical nose was constructed for tests in the Langley full-scale tunnel, and an investigation of the effect of pressure gradient on transition caused by roughness was conducted at Reynolds numbers (based on diameter) up to  $10 \times 10^6$  and at a maximum Mach number of about 0.1.

Tests were made to determine when transition occurred behind various sizes and shapes of roughness placed from  $10^\circ$  to  $30^\circ$  from the stagnation point. The investigation also included studies of the spread of turbulence behind a single particle of roughness, the effect of holes and craters on transition, and the effect of two-dimensional roughness representing ridges and scratches on the nose.

## SYMBOLS

$C_p$	pressure coefficient
$D$	diameter of hemisphere
$d$	roughness width or hole diameter
$h$	depth of hole
$k$	roughness height
$R$	radius of hemisphere
$R_D$	Reynolds number of hemisphere, $\frac{U_\infty D}{\nu}$
$R_d$	Reynolds number based on hole diameter, $\frac{Ud}{\nu}$
$R_k$	Reynolds number of roughness based on roughness height and velocity at top of roughness, $\frac{u_k k}{\nu}$
$R_{\delta^*}$	Reynolds number based on $\delta^*$ , $\frac{U\delta^*}{\nu}$
$R_x$	Reynolds number, $\frac{U_\infty x}{\nu}$
$U$	local velocity outside boundary layer
$U_\infty$	free-stream velocity
$u$	local velocity within boundary layer
$u_k$	value of $u$ at top of roughness
$x$	distance from stagnation point along surface
$y$	distance normal to surface
$\delta^*$	boundary-layer displacement thickness, $\int_0^\infty \left(1 - \frac{u}{U}\right) dy$
$\phi$	position on hemisphere from stagnation point, deg

$\nu$             kinematic viscosity

Subscript:

$t$             when transition is observed

## APPARATUS

### Model

A photograph of the model mounted in the test section of the Langley full-scale tunnel is shown in figure 1. The model consisted of a 10-foot-diameter hollow hemisphere nose mounted on an afterbody 30 feet long. The wall of the nose section was made of polyester plastic reinforced with fiber glass and was approximately  $5/8$  inch thick.

The entire nose was machined to contour and polished to obtain a smooth surface. The surface finish of the nose was from 5 to 7 micro-inches rms as determined by a Profilometer, and a careful inspection of the quadrant used for the tests did not reveal any protuberances over 0.002 inch high.

### Instrumentation

Pressure orifices.- In order to obtain the pressure distribution over the nose, pressure orifices 0.010 inch in diameter were installed every  $10^\circ$  on the horizontal and vertical meridian lines of the hemisphere. Two other pressure orifices were made in the wall of the nose at the  $30^\circ$  stations on opposite sides of the stagnation point. The  $30^\circ$  station was used in order to obtain high sensitivity to small changes in the position of the stagnation point. These orifices were  $1/8$  inch in diameter and were instrumented with electrical pressure pickups as close as possible to the surface in order to obtain maximum frequency response. The output of these pressure pickups was amplified and simultaneously recorded on an oscillograph.

Hot-wire equipment.- Hot-wire anemometers were used to detect turbulence in the boundary layer for all tests of the effects of roughness. The hot wire was a 0.0003-inch-diameter tungsten wire about 0.08 inch long and was mounted in a probe like that shown in figure 2. The hot-wire heating current was supplied by a constant-temperature hot-wire amplifier (described in ref. 7) which has a response good up to about 40,000 cycles per second. Two probes were used simultaneously for tests of the effects of roughness, and the outputs of the two hot-wire amplifiers were viewed on a dual-trace oscilloscope. Pictures of the traces were taken on 35-millimeter film with an oscilloscope camera.

## TESTS

### Basic Flow Studies

Several preliminary tests were made to establish the flow conditions on the smooth nose prior to the roughness tests. The body was first aligned with the tunnel air stream by comparison of the pressures measured by the static-pressure orifices in the nose. Then the pressure distribution over the nose was measured at velocities from 45 feet per second to 150 feet per second. During these tests the pressure fluctuations at the electrical pressure pickups were recorded in order to investigate possible sources of disturbances in the boundary layer. A sublimation flow visualization technique was used to observe natural transition of the boundary layer on the smooth nose. A saturated solution of naphthalene was sprayed on the nose, and the evaporation of the coating was observed as the tunnel speed was increased to 150 feet per second.

### Roughness Tests

Tests were made to determine the effect of two-dimensional and three-dimensional roughness on boundary-layer transition on the hemispherical nose.

For these tests, a hot-wire probe was placed downstream of the roughness, and photographs of the oscilloscope traces were taken as the free-stream velocity was increased. From these observations the value of  $R_{k,t}$  for three-dimensional particles was obtained for various roughness configurations.

In order to find the effect of the shape of the roughness on  $R_{k,t}$ , particles with a height-to-width ratio ( $k/d$ ) of from 0.12 to 4.0 were tested at the  $30^\circ$  station on the nose. These particles included spheres, cylinders, grains of Carborundum, rimmed craters, and rectangular shapes. For tests of the effects of size and position of the roughness, spheres from 0.018-inch to 0.062-inch diameter were placed at stations  $10^\circ$ ,  $20^\circ$ , and  $30^\circ$  from the stagnation point and the  $R_{k,t}$  was determined. Tests of the effect of interaction between particles were made by finding  $R_{k,t}$  for a patch of roughness and then removing all but one particle and redetermining  $R_{k,t}$ . In applying the roughness in patches, care was taken to space the roughness particles so that ridges of tightly packed particles were not formed. The spread of turbulence behind a particle at the  $10^\circ$ ,  $20^\circ$ , and  $30^\circ$  stations was also measured.

Limited tests of the effects of two-dimensional types of roughness were made with wire and scratch types of roughness. Round wires covering one quadrant of the nose were placed normal to the flow at the  $10^\circ$ ,  $20^\circ$ , and  $30^\circ$  stations, and a hot wire was placed behind the wires at the  $40^\circ$  station. Tests were made to determine the velocity at which the first bursts of turbulence occurred at the hot wire. The velocity for transition at the  $20^\circ$  station was also determined for one case. Two-dimensional scratches with raised edges were tested at various orientations to the local flow direction. Cross-section views of typical scratch and crater types of roughness are shown in figure 3.

## RESULTS AND DISCUSSION

### Basic Flow Studies

The pressure distribution over the hemispherical nose of the test model at  $R_D = 9.6 \times 10^6$ , as obtained with the static-pressure orifices, is shown in figure 4. The pressure distribution was essentially the same at all other test speeds. The velocity over the upper right-hand quadrant of the nose, obtained from the average pressure at the top and right side, is shown in figure 5. This quadrant of the nose was used for all roughness tests. As expected, the velocity distribution over the hemispherical nose of the model was nearly the same as the theoretical distribution over a sphere.

The instantaneous position of the stagnation point was obtained by a comparison of the pressures at the orifices instrumented with electrical pressure pickups. By subtracting the pressure at one orifice from the pressure at the other orifice recorded at the same time, the position of the stagnation point relative to these orifices could be found, and fluctuations in pressure due to variations in free-stream speed were cancelled. The equation used for position of the stagnation point was:

$$\beta = \frac{6.37}{\sin 30^\circ \cos 30^\circ} \left( \frac{P_1 - P_2}{q} \right)$$

where

- $\beta$  position of the stagnation point
- $P_1, P_2$  pressures at the orifices
- $q$  average free-stream dynamic pressure

Figure 6 shows a record of the stagnation-point position at two of the highest speeds used in the tests. Because of the small amount of shift in the stagnation point, the boundary layer was probably unaffected by these disturbances.

A photograph of the results of the naphthalene flow visualization is shown in figure 7. For comparison purposes several particles of roughness were placed in the lower quadrant of the nose, and these particles show transition wedges; but the upper quadrant, which was used in all subsequent roughness tests, showed essentially laminar flow back to the  $90^\circ$  station.

It was thought that there was a possibility that disturbances in the boundary layer caused by the Görtler type of instability at the stagnation point might cause premature transition at high Reynolds numbers. Inasmuch as the boundary layer was essentially laminar back to the  $90^\circ$  station on the smooth nose, the results of these tests indicate that the effects of any Görtler type of instability at the stagnation point were not significant at the Reynolds numbers tested.

#### Roughness Studies

Determination of  $R_{k,t}$ . - In references 1 to 6 it was found that the roughness Reynolds numbers showed good correlation with boundary-layer transition produced by three-dimensional roughness. In order to calculate  $R_k$ , it is necessary to know the velocity at the top of the roughness particle; therefore, the boundary-layer profile as well as the local velocity outside the boundary layer must be known. Since the velocity distribution over the nose of the test model was essentially the same as the theoretical distribution on a sphere, especially at stations near the stagnation point, the velocity distribution in the boundary layer on the model nose could be adequately determined by using the theoretical boundary layer at the corresponding station on a sphere. Figure 8 shows the velocity distribution in the boundary layer on a sphere from reference 8 which was used in the calculation of  $R_k$  values.

In the determination of  $R_k$  it is essential that the height of the particle be very accurately determined, since  $R_k$  varies as the square of the particle height when the particle is in the linear portion of the boundary layer. Since  $R_k$  is very sensitive to roughness height, some of the scatter shown in the values obtained for  $R_{k,t}$  may be attributable to errors in determining the height of the particle.

Figure 9, which is typical of the plots used in analyzing the data, shows the relative amount of time that the boundary layer is turbulent

plotted against the  $R_k$  of a spherical roughness particle on the hemispherical nose for various locations of the hot wire. From this figure it can be seen that the first bursts of turbulence in the boundary layer occur at all downstream stations at essentially the same  $R_k$ . ( $R_k = 635$  in this case.) Similar plots for other particles also showed that the  $R_k$  at which the first bursts of turbulence were observed was independent of the downstream position of observation. Also, plots of the  $R_k$  for the first bursts of turbulence against the distance of the observation point behind the particle showed that this  $R_k$  was independent of observation position since there was no obvious trend. Therefore, the value of  $R_k$  at which the first bursts of turbulence were observed was taken as the critical  $R_k$  for transition ( $R_{k,t}$ ).

Figure 9 also shows that for higher free-stream velocities the relative amount of time that the boundary layer is turbulent increases as the observation point is moved downstream. This confirms previous concepts of transition given in reference 9 in which turbulent spots originate at the particle and grow in size as they progress downstream until they finally coalesce to form a completely turbulent boundary layer at some station downstream of the particle.

Although occasional random bursts of turbulence occurred on the smooth nose, the use of one hot wire behind the particle and a comparison hot wire on a smooth section of the nose enabled fairly accurate determination of the tunnel speed at which first bursts of turbulence from the roughness occurred. The values given for the relative amount of time that the boundary layer was turbulent are not as accurate for higher values since they were obtained by visual observations of the oscilloscope screen. All measurements given herein of the relative amount of time that the boundary layer was turbulent are corrected for the occasional turbulent bursts observed by the comparison hot wire at the same time.

Three-dimensional particles.— Initial studies with roughness particles of different types showed a large effect of shape on  $R_{k,t}$  for single three-dimensional roughness particles. However,  $R_{k,t}$  showed a definite trend with the height-to-width ratio ( $k/d$ ) of the particle. This trend is similar to that shown in reference 1 for two-dimensional flow. Figure 10 shows the variation of  $R_{k,t}$  with  $k/d$  for roughness which is immersed in the boundary layer and which ranges from single Carborundum grains to rimmed craters. Test points for the crater type of roughness are identified in figure 10 by flagged symbols and the unflagged symbols represent  $R_{k,t}$  for grains, spheres, poles, and brick-shaped roughnesses. This figure shows that the rimmed crater type of roughness has about the same  $R_{k,t}$  as three-dimensional particles with the same  $k/d$ . The spread

of the data points can be mostly attributed to inaccuracies in measuring the height of the roughness particle and in determining the exact speed at which the first bursts of turbulence occurred in the boundary layer.

In order to eliminate the effect of the shape of the roughness, spherical roughness particles were used in determining the effects of position and size of the roughness on  $R_{k,t}$ . The results of these tests are presented in figure 11 for roughness at the  $10^\circ$ ,  $20^\circ$ , and  $30^\circ$  stations. The values of  $k/\delta^*$  in the range tested (1.15 to 3.55) all represent particles within the boundary-layer thickness, with the highest approximately at the top of the boundary layer. Only particles within the boundary layer were tested, since it was shown in reference 4 that this was the most critical condition and that particles which protruded through the boundary layer had higher values of  $R_{k,t}$ . As can be seen from figure 11,  $R_{k,t}$  is not affected by  $k/\delta^*$  for values that are within the boundary-layer thickness ( $k/\delta^* < 3.6$ ). Figure 11 shows that  $R_{k,t}$  was from 530 to 766 for spherical roughness particles at all stations tested on the nose, which compares favorably with  $R_{k,t}$  from 490 to 760 found in reference 5 for spherical particles on a flat plate. The three positions tested are in a moderate to large stabilizing pressure gradient and therefore show that  $R_{k,t}$  is unaffected by stabilizing pressure gradients in three-dimensional flow.

Tests were made to determine whether interaction between closely spaced particles, such as those found in patches of roughness, changed the value of  $R_{k,t}$ . The results of these tests are shown in table I. As can be seen, no appreciable effect was found to be caused by interaction between the particles.

A limited survey of the area behind a single particle at the  $10^\circ$ ,  $20^\circ$ , and  $30^\circ$  stations on the hemisphere was made with hot-wire anemometers to determine the spread of turbulence. Figure 12 shows a sample plot of the relative amount of time the boundary layer is turbulent behind a 0.040-inch spherical particle at the  $30^\circ$  station on the nose. The two survey stations show that the half-angle of the wedge of maximum spread of turbulence is  $8.6^\circ$ . The wedge half-angle behind a roughness particle at the  $10^\circ$  and  $20^\circ$  stations on the hemisphere were measured to be  $8.9^\circ$  and  $8.6^\circ$ , respectively. These angles compare favorably with the half-angle of the wedge of turbulence on a flat plate given in reference 9 (from  $8.6^\circ$  to  $10^\circ$ ).

Two-dimensional roughness.— Transition behind two-dimensional roughness on the hemisphere was found to occur in much the same way as on a flat plate. Figure 13 shows the relative amount of time that the boundary layer was turbulent at two stations downstream of a two-dimensional roughness at the  $10^\circ$  station on the hemispherical nose. The two curves

show that the first bursts of turbulence (transition) occur originally at a station far downstream of the roughness and then at a station closer to the roughness at a higher free-stream velocity. Evidently, with two-dimensional roughness on the hemispherical nose, transition is caused downstream of the roughness location and progresses forward as the free-stream velocity is increased as it does with two-dimensional roughness on a flat plate. This method of transition is in contrast to the method previously observed for three-dimensional roughness particles where transition occurred at all downstream stations simultaneously.

Only a limited number of tests were made with two-dimensional roughnesses in order to obtain a general idea of the sizes of roughness necessary to cause transition. All tests except one were made to determine when transition occurred at the  $40^\circ$  station, and since the limited amount of data prevented the formation of a complete picture of transition behind two-dimensional roughness, the data are given in tabular form in table II in addition to the curves of figure 14.

In figure 14 the results obtained on the hemispherical nose are compared with results on a flat plate from reference 10. It is believed that transition behind two-dimensional roughness on a hemisphere is related to the local boundary-layer conditions; therefore, a Reynolds number based on local boundary-layer conditions,  $R_{\delta^*}$ , is used in figure 14 instead of  $R_x$  which is normally used for correlating transition results from two-dimensional roughness on a flat plate. As can be seen from the curves, the  $k/\delta^*$  required to cause transition at a fixed location increases as the roughness is moved forward on the nose.

Holes and scratches.— A few tests were made to determine the effects of holes such as pressure orifices on transition of the boundary layer. Figure 15 shows the transition Reynolds number based on velocity outside the boundary layer and on hole diameter against ratio of hole depth to diameter for holes of 0.345-inch diameter at the  $30^\circ$  station on the hemisphere. As might be expected, the transition Reynolds number for the hole approaches a constant value as the depth of the hole increases beyond the point where the bottom of the hole affects the flow at the entrance to the hole. A few tests were made to determine the effect of various hole diameters and positions on the hemisphere. Figure 16 shows the transition Reynolds number for the deepest holes tested. The transition Reynolds numbers obtained ranged from 11,700 to 13,400 and showed practically no effects due to the size or position of the hole.

These tests were made with no air flow through the hole and cannot be expected to apply to holes that have air flow through them. For example, during the naphthalene flow visualization studies, a transition wedge was observed behind an orifice of 1/8-inch diameter that was open to the inside of the model, but the wedge did not appear later when the orifice was plugged on the inside to prevent air leakage.

A limited investigation of the effect of scratches with raised edges on boundary-layer transition was made with scratches at the  $30^\circ$  station on the hemisphere and at various angles to the flow. The scratches were made in the surface of the hemisphere with a penknife and were about 10 inches long. Table III gives the values of  $(k/\delta^*)_t$  and  $R_{k,t}$  for three orientations of the scratch, where  $k$  is the height of the ridge as shown in figure 3. The values obtained for  $(k/\delta^*)_t$  at  $90^\circ$  and  $45^\circ$  to the flow show that the scratch acts in the same way as two-dimensional roughness, whereas the  $R_{k,t}$  for a scratch at  $0^\circ$  to the flow is comparable to that for three-dimensional roughness.

### CONCLUSIONS

An investigation of the effect of a highly favorable pressure gradient on transition caused by roughness on a 10-foot-diameter hemispherical nose in the Langley full-scale tunnel leads to the following conclusions:

1. For roughness which is immersed in the boundary layer, the critical roughness Reynolds number based on height of the roughness and velocity at the top of a three-dimensional roughness particle is nearly constant for a given shape of roughness and is independent of position of the roughness on the hemisphere. The range of critical roughness Reynolds number from 530 to 766 obtained in this investigation for spherical roughness particles on the 10-foot-diameter hemisphere agrees well with the critical roughness Reynolds numbers found in two-dimensional tests on a flat plate and on an airfoil.
2. The interaction between closely spaced particles, such as in a patch of roughness, has no significant effect on the critical roughness Reynolds number for transition of the roughness based on roughness height and velocity at top of roughness.
3. The ratio of height to width of a three-dimensional roughness particle submerged in the boundary layer has a large effect on the critical Reynolds number for transition and the height-to-width ratio of the particle showed a definite trend with the critical Reynolds number for transition for all roughness sizes and positions on the hemisphere.
4. For two-dimensional roughness the position of the roughness on the hemisphere has a large effect on the ratio of roughness height to boundary-layer displacement thickness at which transition occurs at the  $40^\circ$  station at a given Reynolds number of the hemisphere.

5. No disturbances were found in the boundary layer behind a three-dimensional particle until the critical roughness Reynolds number was reached. Turbulent spots were then produced in the boundary layer essentially at the particle, and the relative amount of time the boundary layer was turbulent increased rapidly with an increase in free-stream velocity. This method of transition is in contrast to the method behind a two-dimensional roughness where the turbulent bursts were observed to occur downstream of the roughness and progressed forward as the free-stream velocity increased. These results are consistent with previous concepts of transition behind roughness elements on a flat plate.

6. The half-angle of the wedge of turbulence measured behind a three-dimensional particle was from  $8.6^\circ$  to  $8.9^\circ$  for particles at the  $10^\circ$ ,  $20^\circ$ , and  $30^\circ$  stations on the hemisphere nose. These values agree well with the  $8.6^\circ$  to  $10^\circ$  given for a flat plate in NACA Rep. 1289.

7. Holes which have a large depth-to-diameter ratio act like three-dimensional roughness and the measured critical Reynolds number, based on diameter of the hole and velocity at the top of the boundary layer, was from 11,700 to 13,400. The critical Reynolds number for deep holes shows little effect from size or position of the hole on the hemisphere. As the ratio of depth to diameter of the hole is reduced, the critical Reynolds number varies in an irregular manner and shows large variations with small differences in the ratio of depth to diameter. Flow of air through the hole will cause transition much below the critical Reynolds number found without flow.

8. Scratches orientated at  $90^\circ$  and  $45^\circ$  to the air flow have approximately the same ratio of roughness height to boundary-layer displacement thickness at which transition occurs as two-dimensional wires in the same position on the hemisphere; however, scratches at  $0^\circ$  relative to the air stream have a critical roughness Reynolds number for transition approximately the same as three-dimensional roughness.

9. Rimmed craters have about the same critical roughness Reynolds number for transition as three-dimensional particles with the same height-to-width ratio.

Langley Research Center,  
National Aeronautics and Space Administration,  
Langley Field, Va., November 4, 1958.

## REFERENCES

1. Loftin, Laurence K., Jr.: Effects of Specific Types of Surface Roughness on Boundary-Layer Transition. NACA WR L-48, 1946. (Formerly NACA ACR L5J29a.)
2. Tani, Itiro, Hama, Ryosuke, and Mituisi, Satosi: On the Permissible Roughness in the Laminar Boundary Layer. Rep. No. 199 (vol. XV, 13), Aero. Res. Inst., Tokyo Imperial Univ., Oct. 1940.
3. Schwartzberg, Milton A., and Braslow, Albert L.: Experimental Study of the Effects of Finite Surface Disturbances and Angle of Attack on the Laminar Boundary Layer of an NACA 64A010 Airfoil With Area Suction. NACA TN 2796, 1952.
4. Von Doenhoff, Albert E., and Horton, Elmer A.: A Low-Speed Experimental Investigation of the Effect of a Sandpaper Type of Roughness on Boundary-Layer Transition. NACA Rep. 1349, 1958. (Supersedes NACA TN 3858.)
5. Klebanoff, P. S., Schubauer, G. B., and Tidstrom, K. D.: Measurements of the Effect of Two-Dimensional and Three-Dimensional Roughness Elements on Boundary-Layer Transition. Jour. Aero. Sci. (Readers' Forum), vol. 22, no. 11, Nov. 1955, pp. 803-804.
6. Braslow, Albert L.: Effect of Distributed Granular-Type Roughness on Boundary-Layer Transition at Supersonic Speeds With and Without Surface Cooling. NACA RM L58A17, 1958.
7. Laurence, James C., and Landes, L. Gene: Auxiliary Equipment and Techniques for Adapting the Constant-Temperature Hot-Wire Anemometer to Specific Problems in Air-Flow Measurements. NACA TN 2843, 1952.
8. Schlichting, Hermann (J. Kestin, trans.): Boundary Layer Theory. McGraw-Hill Book Co., Inc., 1955, pp. 165-167.
9. Schubauer, G. B., and Klebanoff, P. S.: Contributions on the Mechanics of Boundary-Layer Transition. NACA Rep. 1289, 1956. (Supersedes NACA TN 3489.)
10. Dryden, Hugh L.: Review of Published Data on the Effect of Roughness on Transition From Laminar to Turbulent Flow. Jour. Aero. Sci., vol. 20, no. 7, July 1953, pp. 477-482.

TABLE I

ROUGHNESS REYNOLDS NUMBER FOR TRANSITION BY PATCHES OF  
ROUGHNESS AND SINGLE PARTICLES OF ROUGHNESS ON  
A HEMISPHERICAL NOSE

Type of roughness	$R_{k,t}$		Ratio of spacing to diameter of particle for patch
	Single	Patch	
0.018-inch spherical roughness at 30° station	530	471	1.5 - 5
0.030-inch Carborundum at 30° station	342	338	3 - 10
0.019-inch Carborundum at 20° station	359	404	3 - 10

TABLE II

TRANSITION BEHIND TWO-DIMENSIONAL ROUGHNESS ON A 10-FOOT-DIAMETER HEMISPHERICAL NOSE

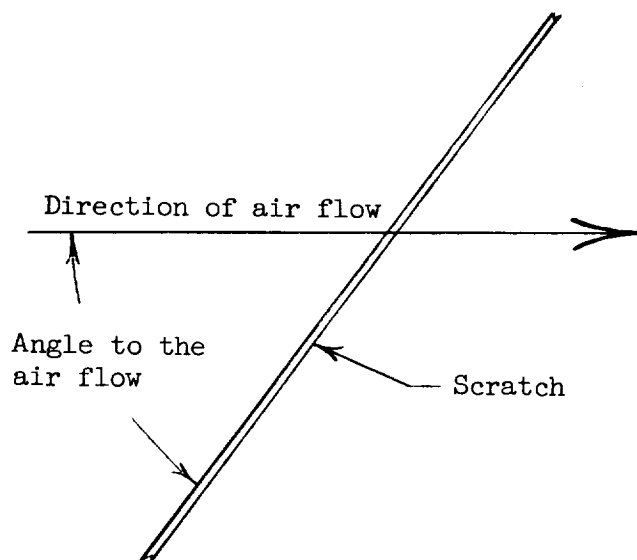
Roughness position, $\phi_k$ , deg	Roughness height, $k$ , in.	Position where transition is observed, $\phi_t$ , deg	$R_D$ when transition is observed, $R_{D,t}$	$\frac{\text{Roughness height}}{\text{Displacement thickness}}, \frac{k}{\delta^*}$	Displacement-thickness Reynolds number at transition point, $\frac{U\delta^*}{\nu}$	Roughness Reynolds number, $\frac{u_k k}{\nu}$
10	0.020	40	$7.30 \times 10^6$	1.30	985	233
	.032		5.41	1.76	850	315
20	0.010	40	8.15	0.68	1,040	155
	.020		4.61	1.02	783	242
	.032		3.45	1.42	678	357
30	0.010	40	7.26	0.62	983	188
	.011		6.97	.67	960	211
	.020		4.16	.94	744	300
10	0.032	20	6.14	1.88	447	368

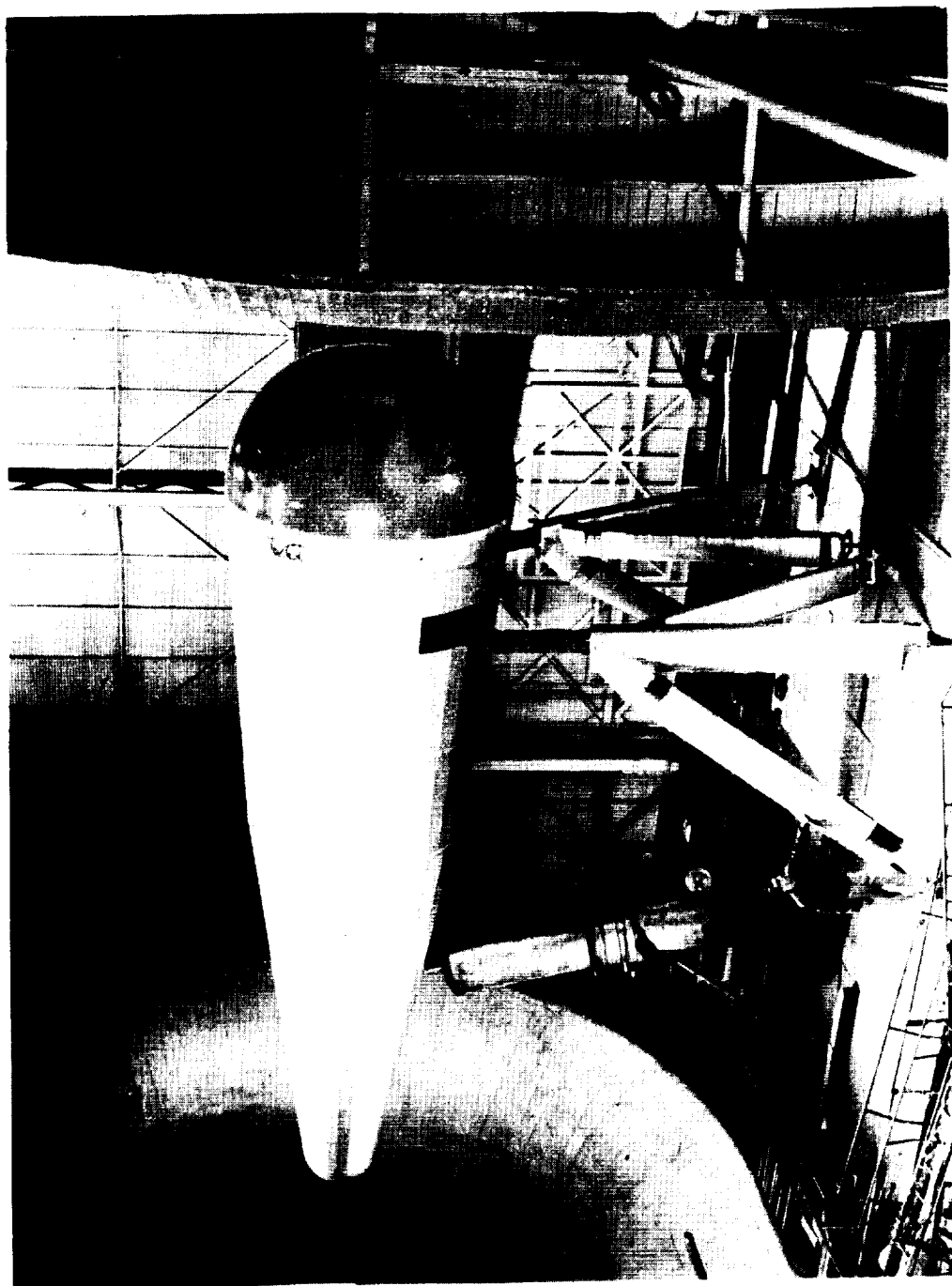
TABLE III

$(k/\delta^*)_t$  AND  $R_{k,t}$  FOR SCRATCH TYPE OF ROUGHNESS AT  
VARIOUS ORIENTATIONS TO THE AIR FLOW

[Scratch at  $30^\circ$  station and hot wire at  $40^\circ$  station  
on the hemisphere]

Angle to the air flow, deg	Height of ridge of scratch, in.	$R_{\delta^*}$ at transition point	$(k/\delta^*)_t$ at scratch	$R_{k,t}$ of scratch
90	0.011	960	0.67	211
45	.010	915	.58	154
0	.020	1,007	1.28	680

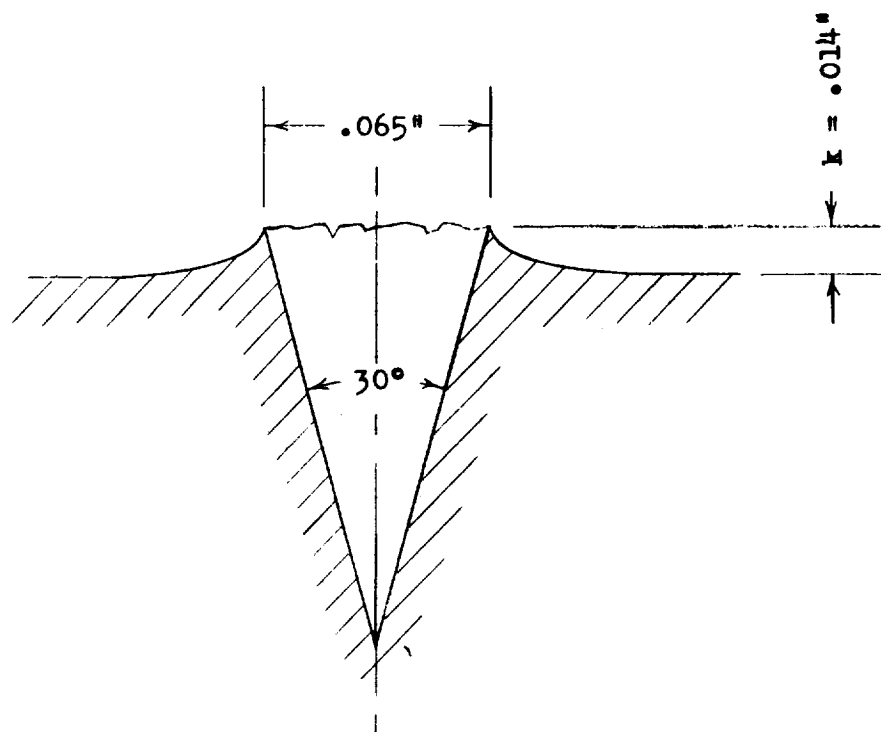




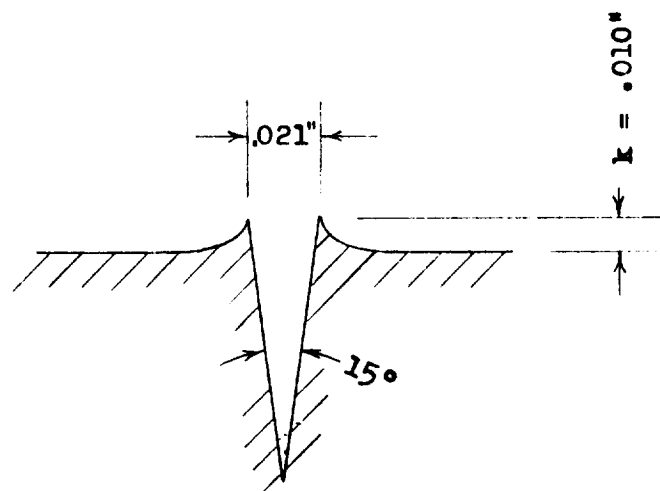
L-57-5549  
Figure 1.- Photograph of 10-foot-diameter hemispherical nose with afterbody in test section of  
the Langley full-scale tunnel.



Figure 2.- Photograph of hot-wire holder. L-90896



Crater



Scratch

Figure 3.- Cross-section view of typical crater and scratch types of roughness.

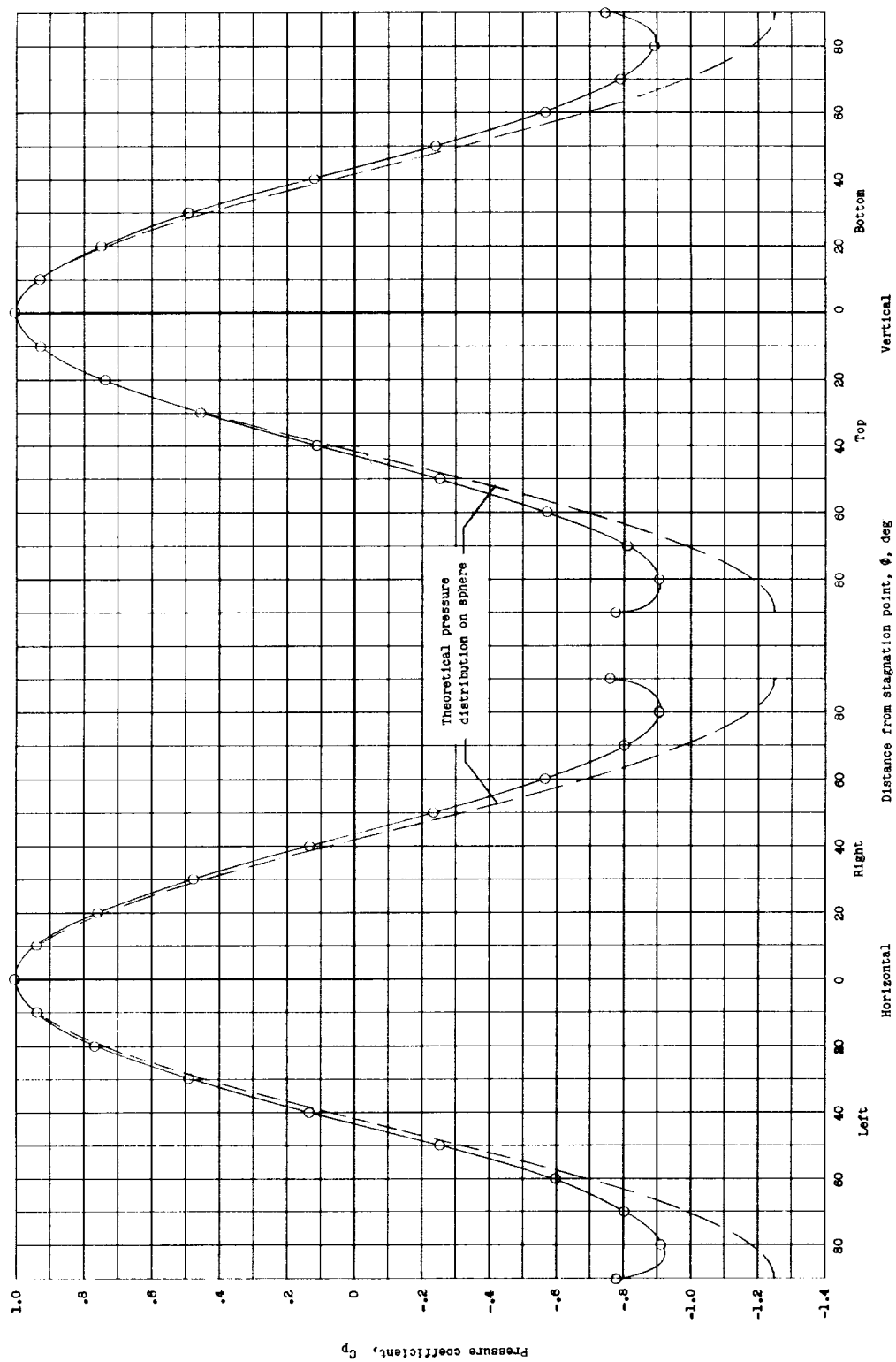


Figure 4.- Pressure distribution on the 10-foot-diameter hemisphere at  $R_D = 9.6 \times 10^6$ .

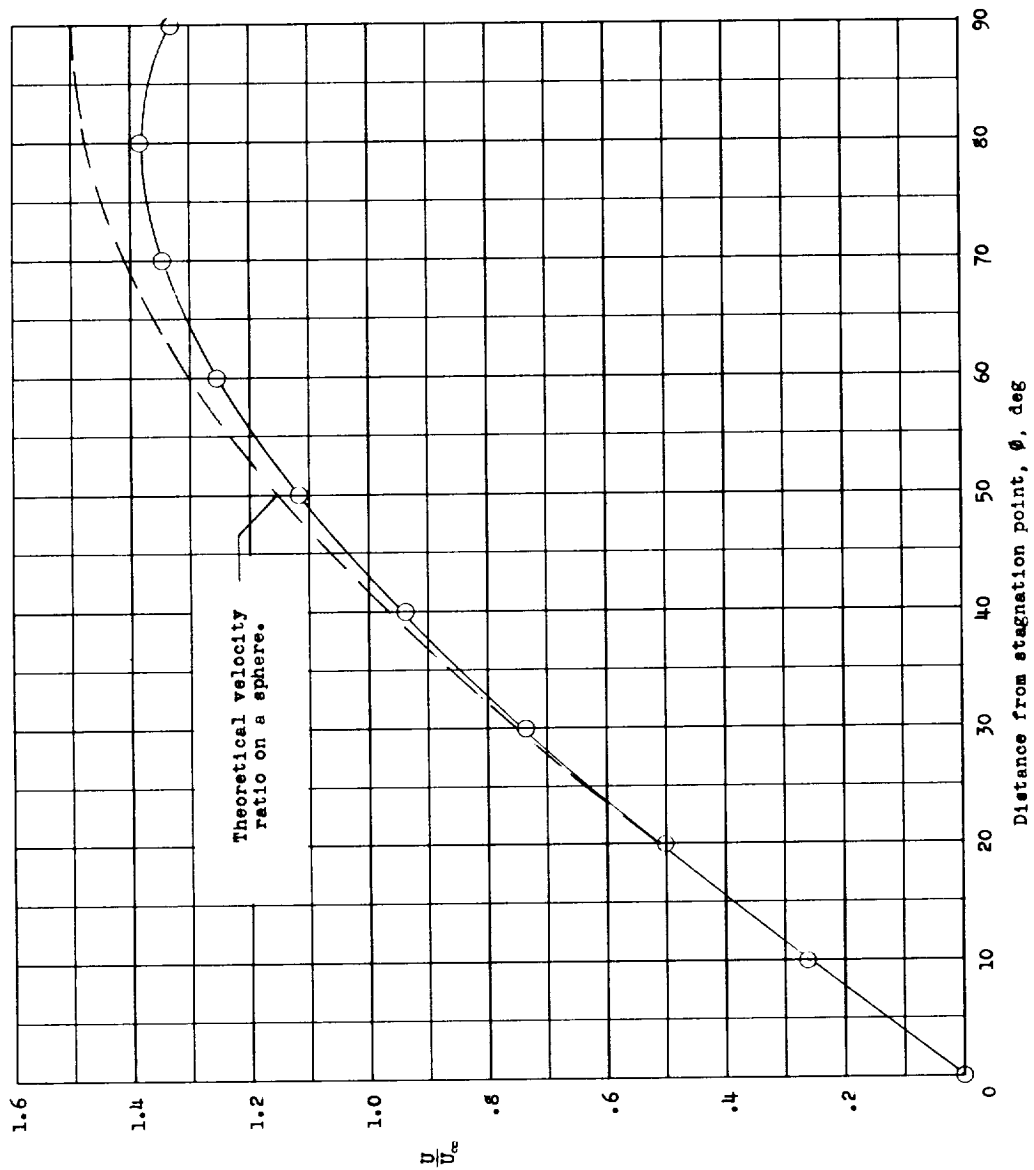


Figure 5.- Nondimensional velocity distribution on the 10-foot-diameter hemisphere at  $Re = 9.6 \times 10^6$ .

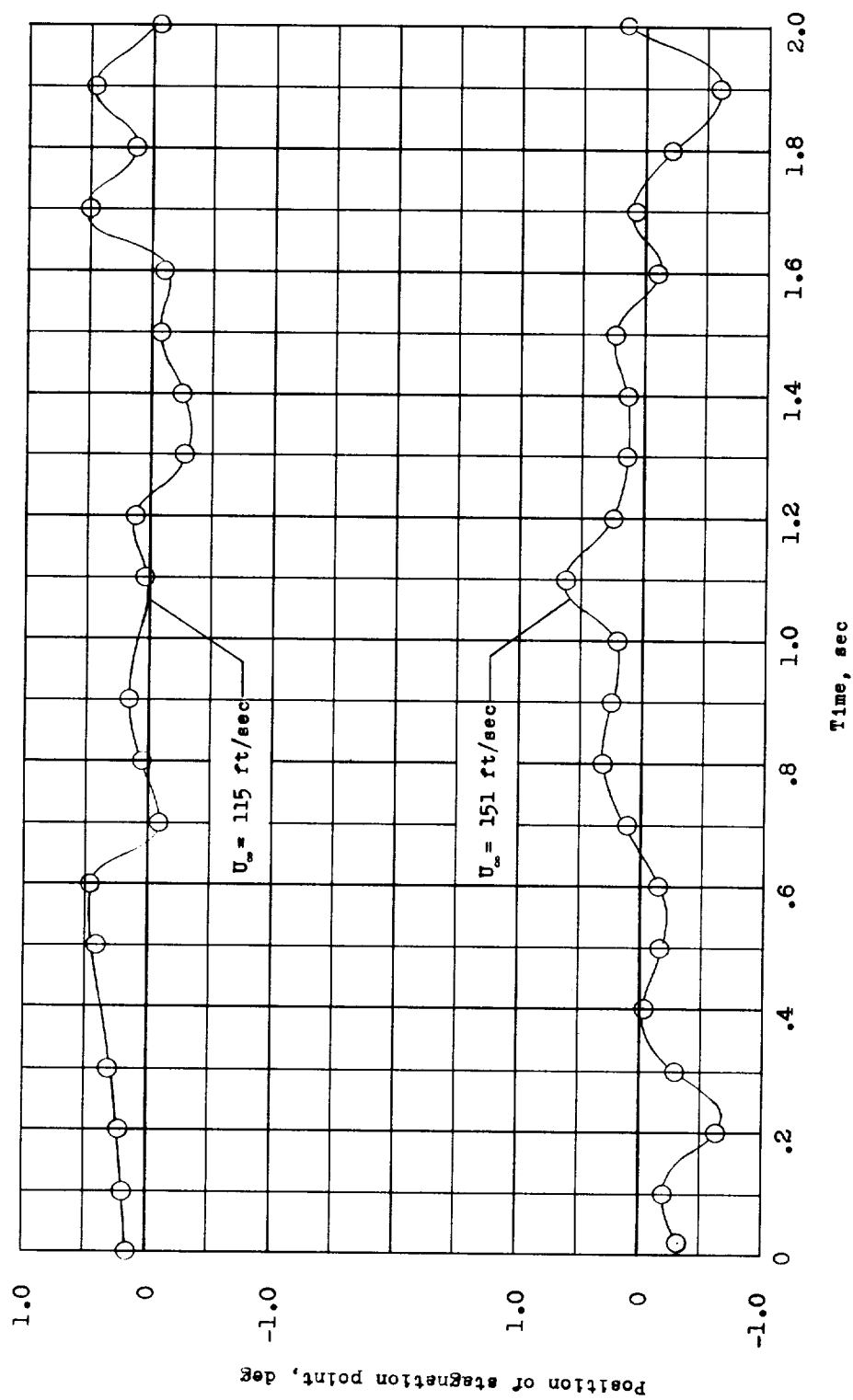


Figure 6.- Stagnation-point shift.



L-58-155a  
Figure 7.- Photograph of transition pattern on the hemisphere as shown by naphthalene at  
 $R_D = 7.3 \times 10^6$ .

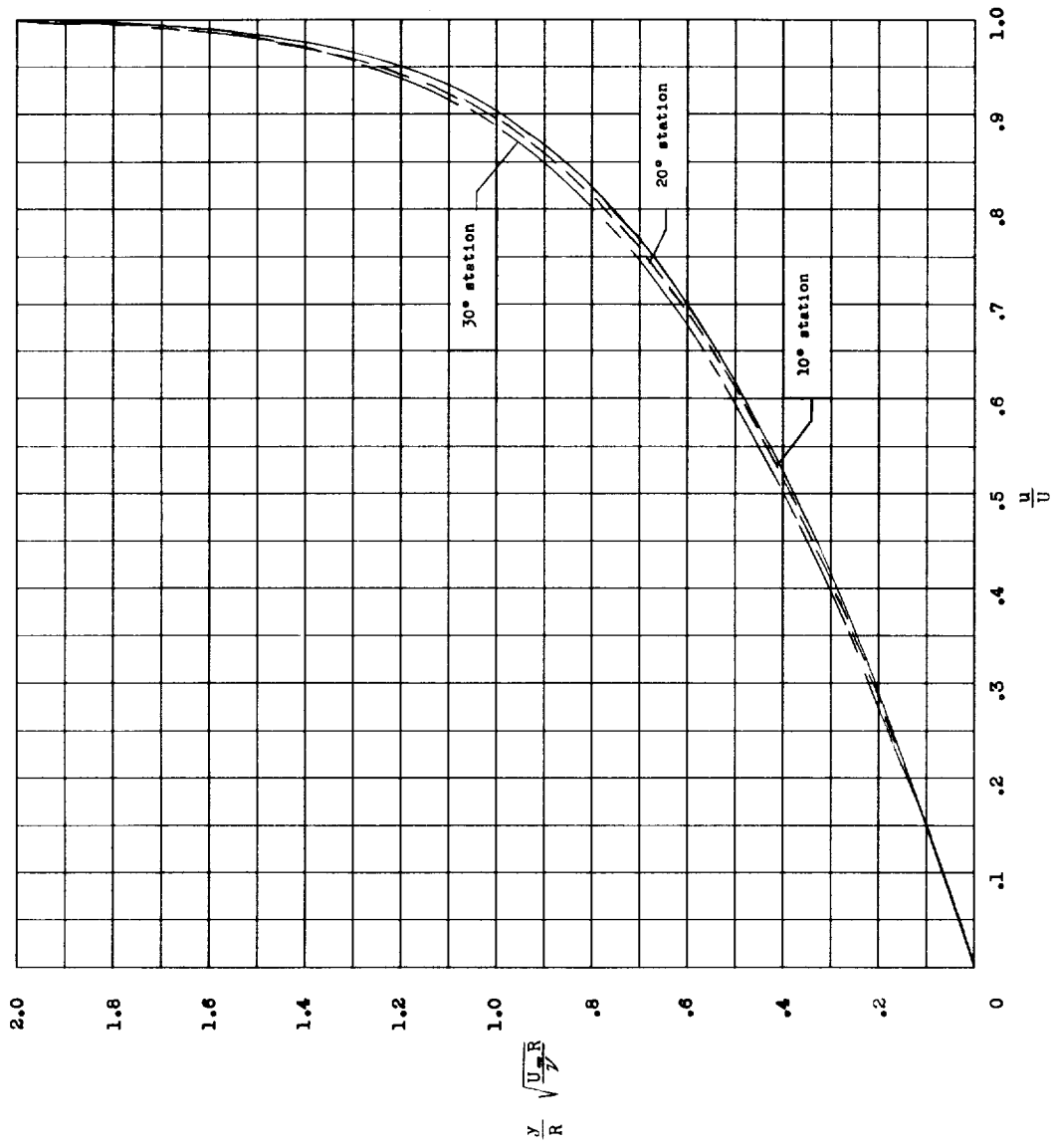


Figure 8.- Nondimensional velocity distribution in the boundary layer on a sphere.

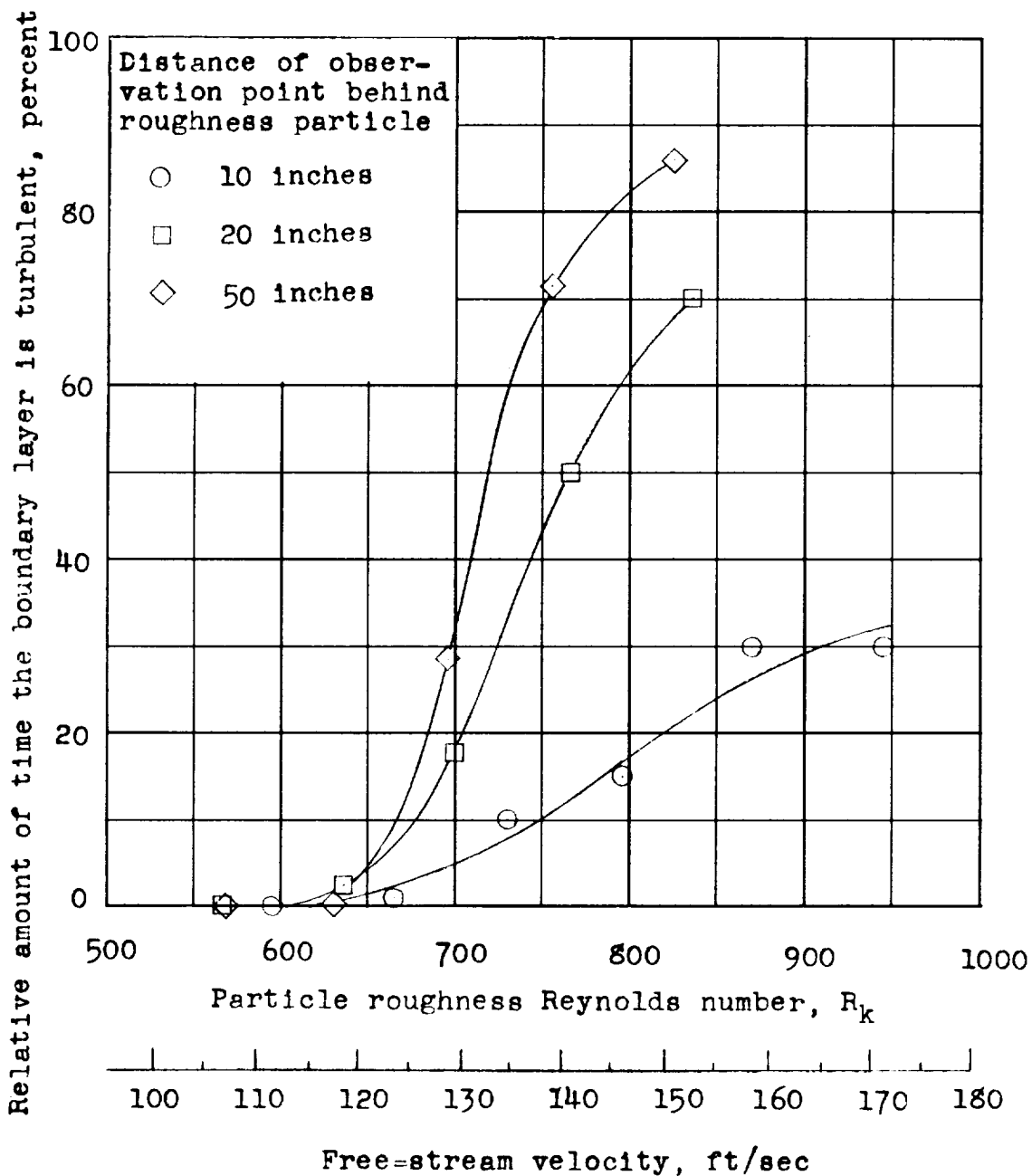


Figure 9.- Relative amount of time the boundary layer is turbulent at various distances behind a 0.040-inch spherical particle at the  $10^0$  station.

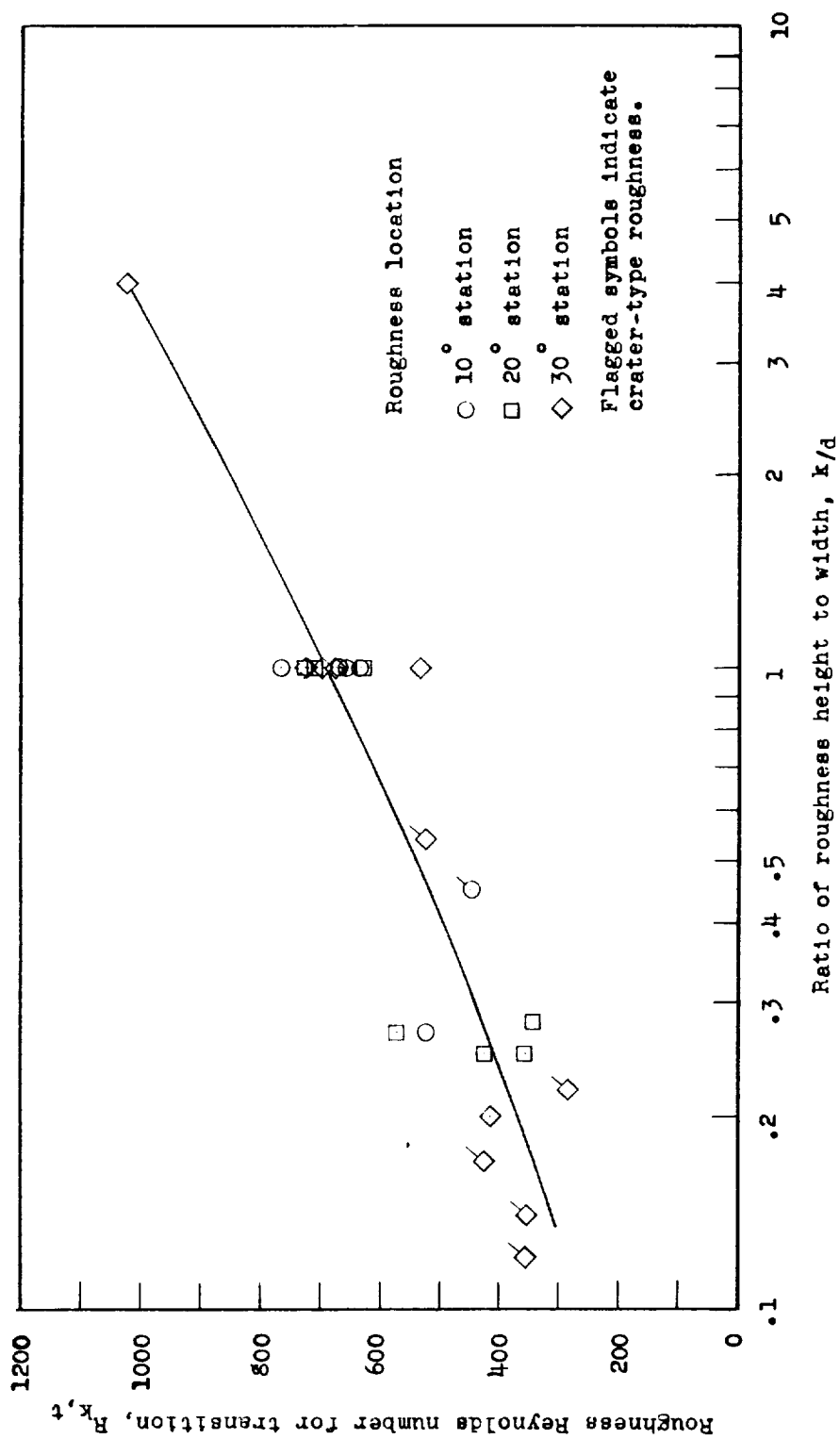


Figure 10.- Effect of shape of roughness particle on critical roughness Reynolds number for transition on a hemispherical nose.

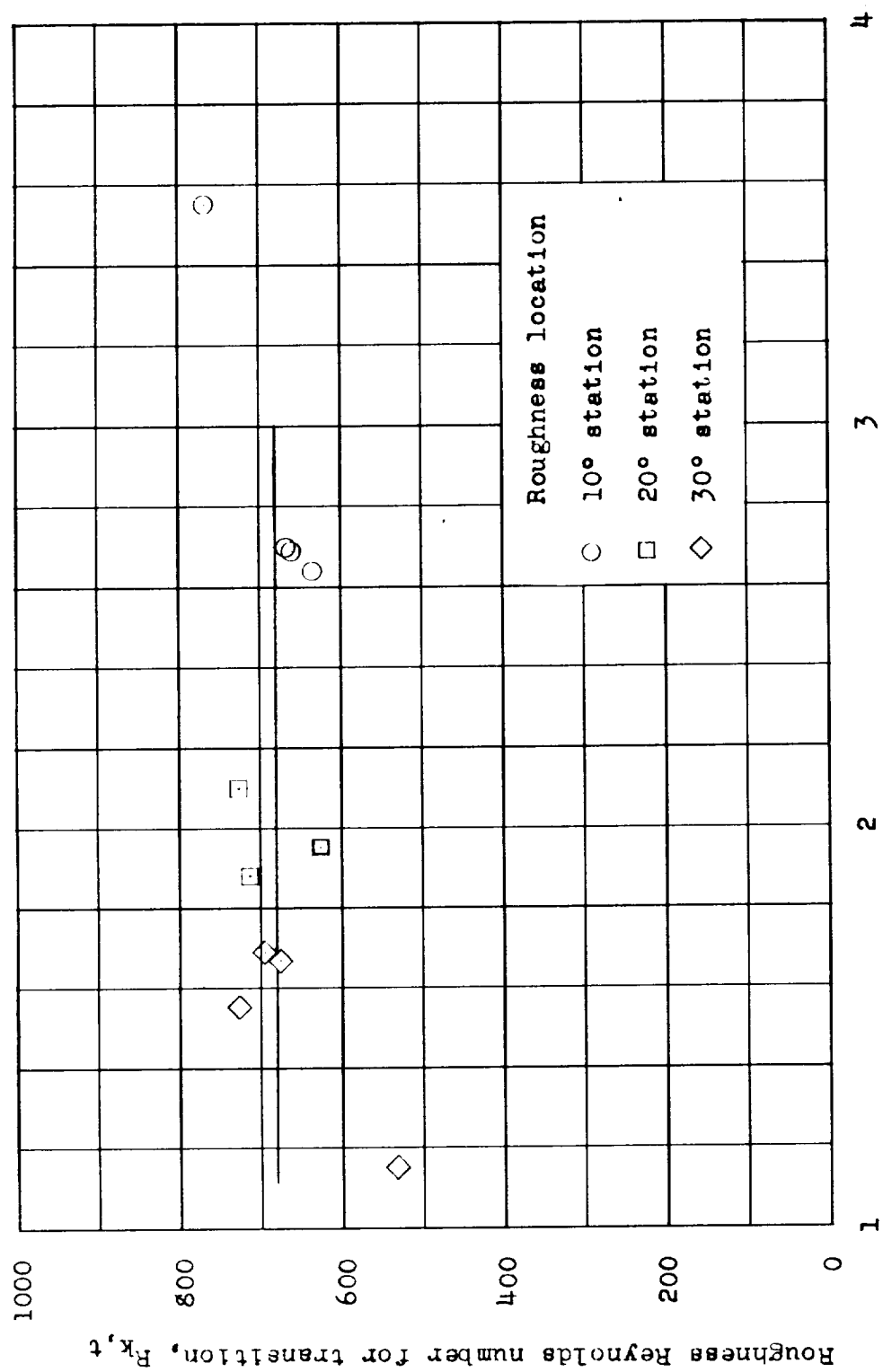


Figure 11.- Transition Reynolds number for spherical roughness particles on a hemispherical nose.

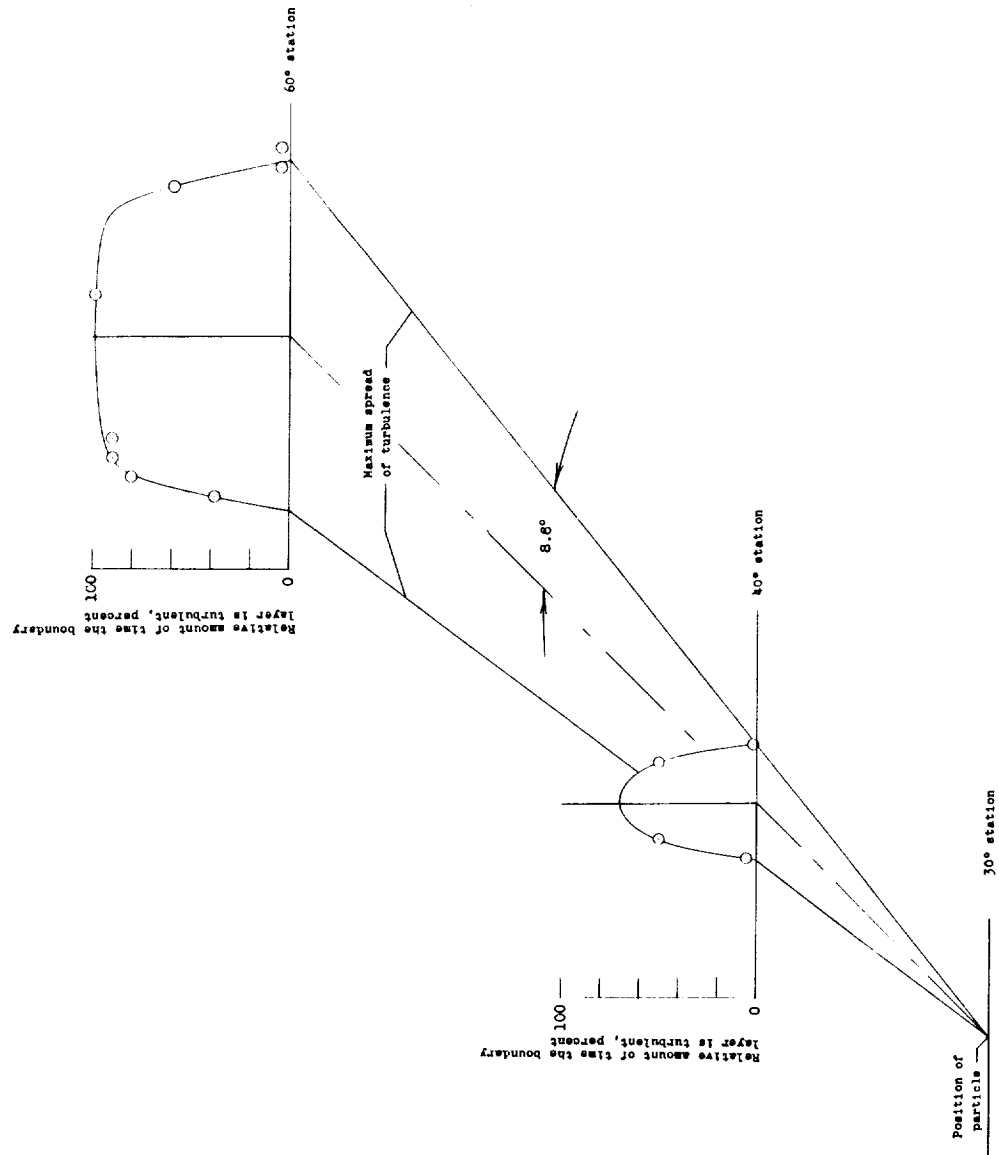


Figure 12.- Spread angle of wedge of turbulence behind a 0.040-inch spherical particle at the 30° station.  $R_k = 830$ ;  $R_D = 5.2 \times 106$ .

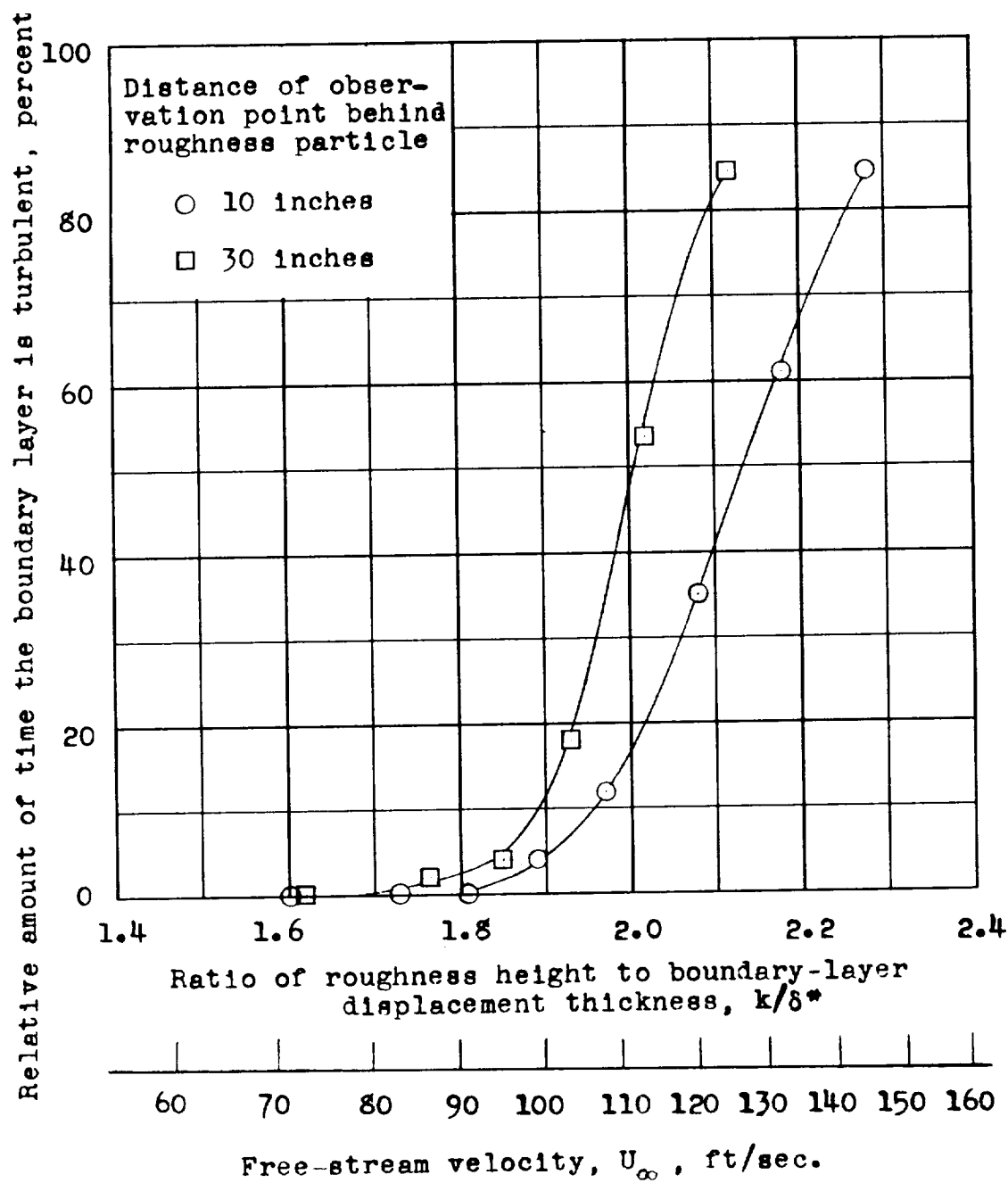


Figure 13.- Relative amount of time the boundary layer is turbulent at various distances behind 0.032-inch two-dimensional roughness at the  $10^\circ$  station.

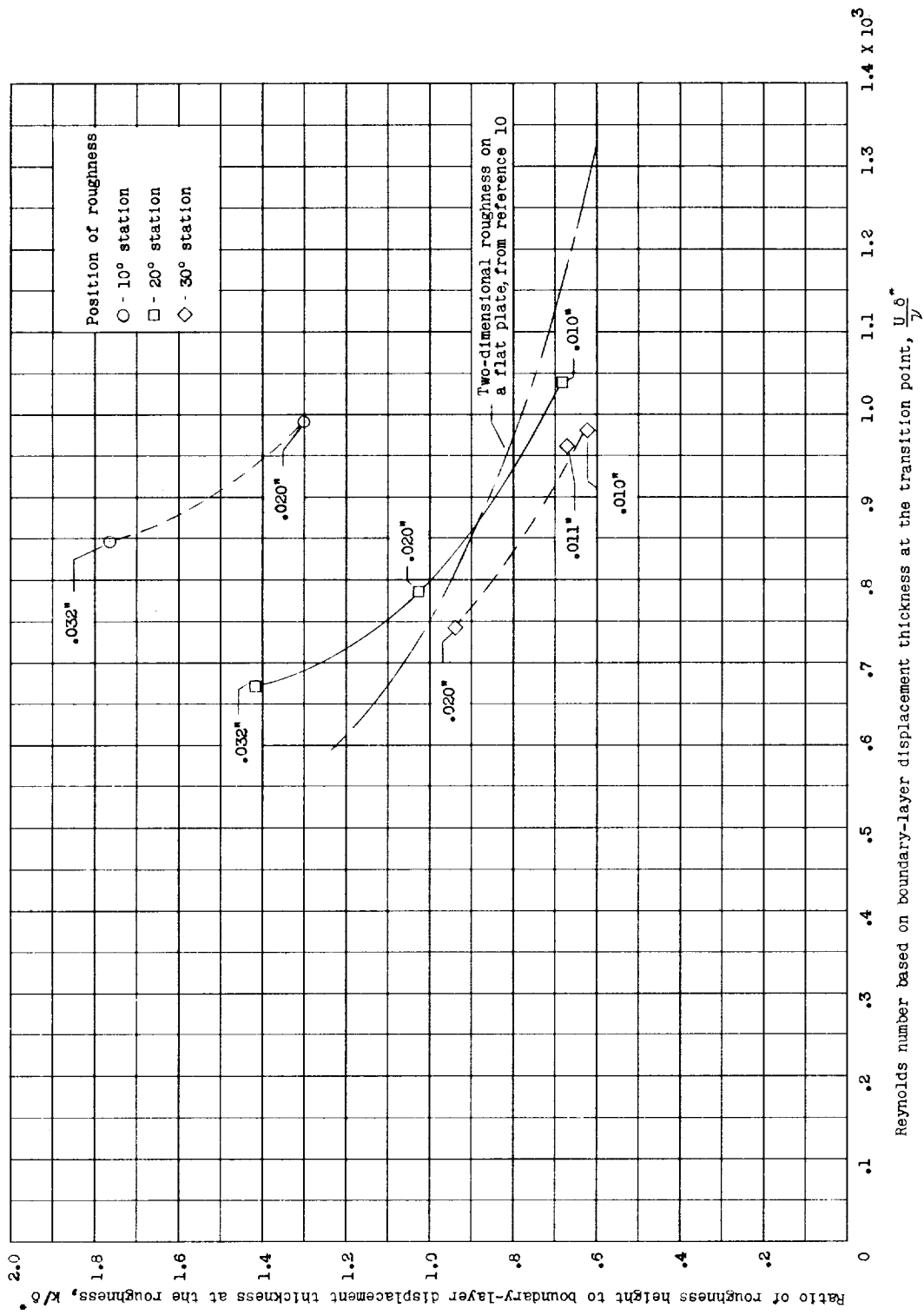


Figure 14.- Reynolds number based on  $\delta^*$  at the transition point for transition occurring at the 40° station behind two-dimensional roughness on a hemisphere.

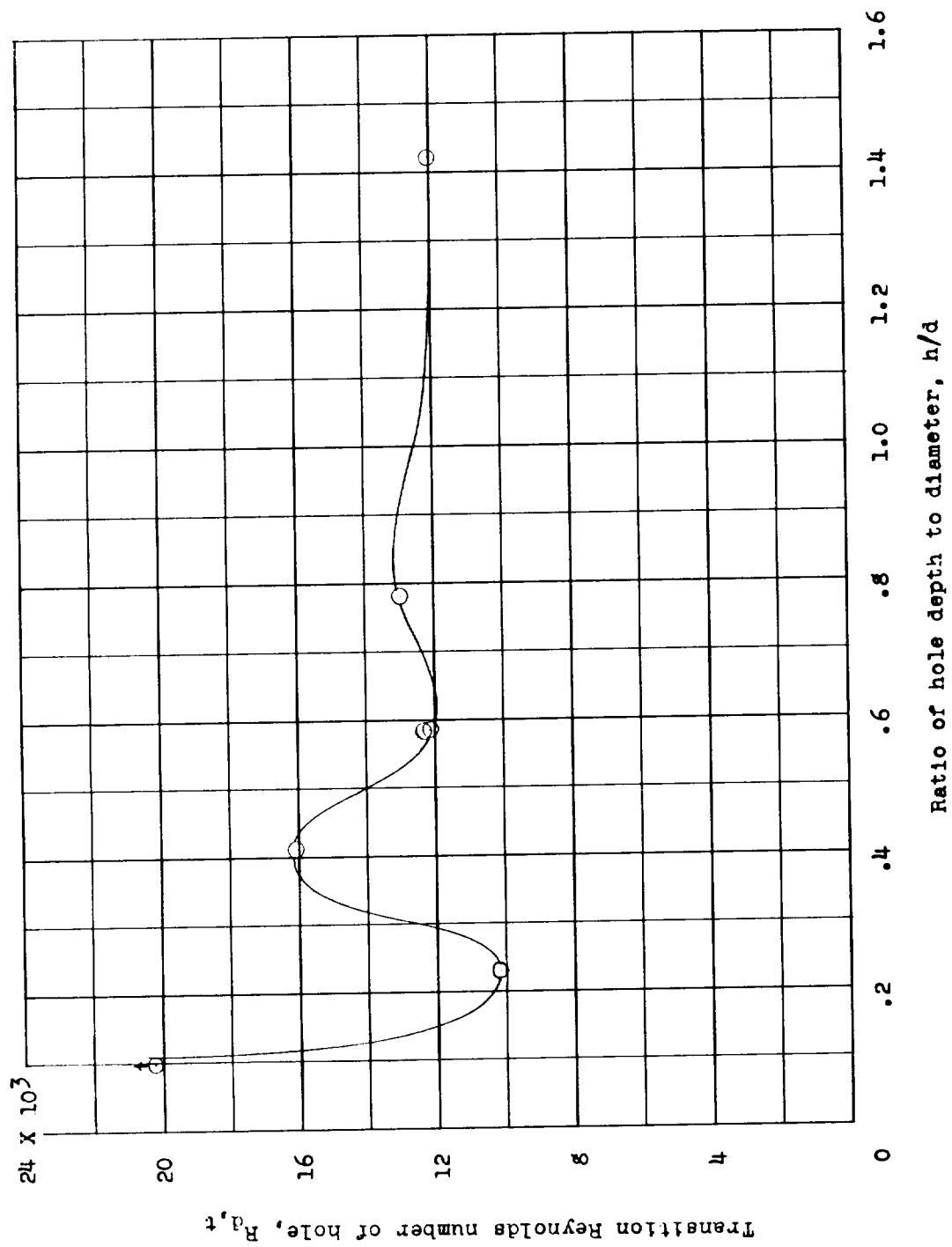


Figure 15.- Transition Reynolds number based on hole diameter and velocity at top of boundary layer for 0.345-inch-diameter holes at 30° station.

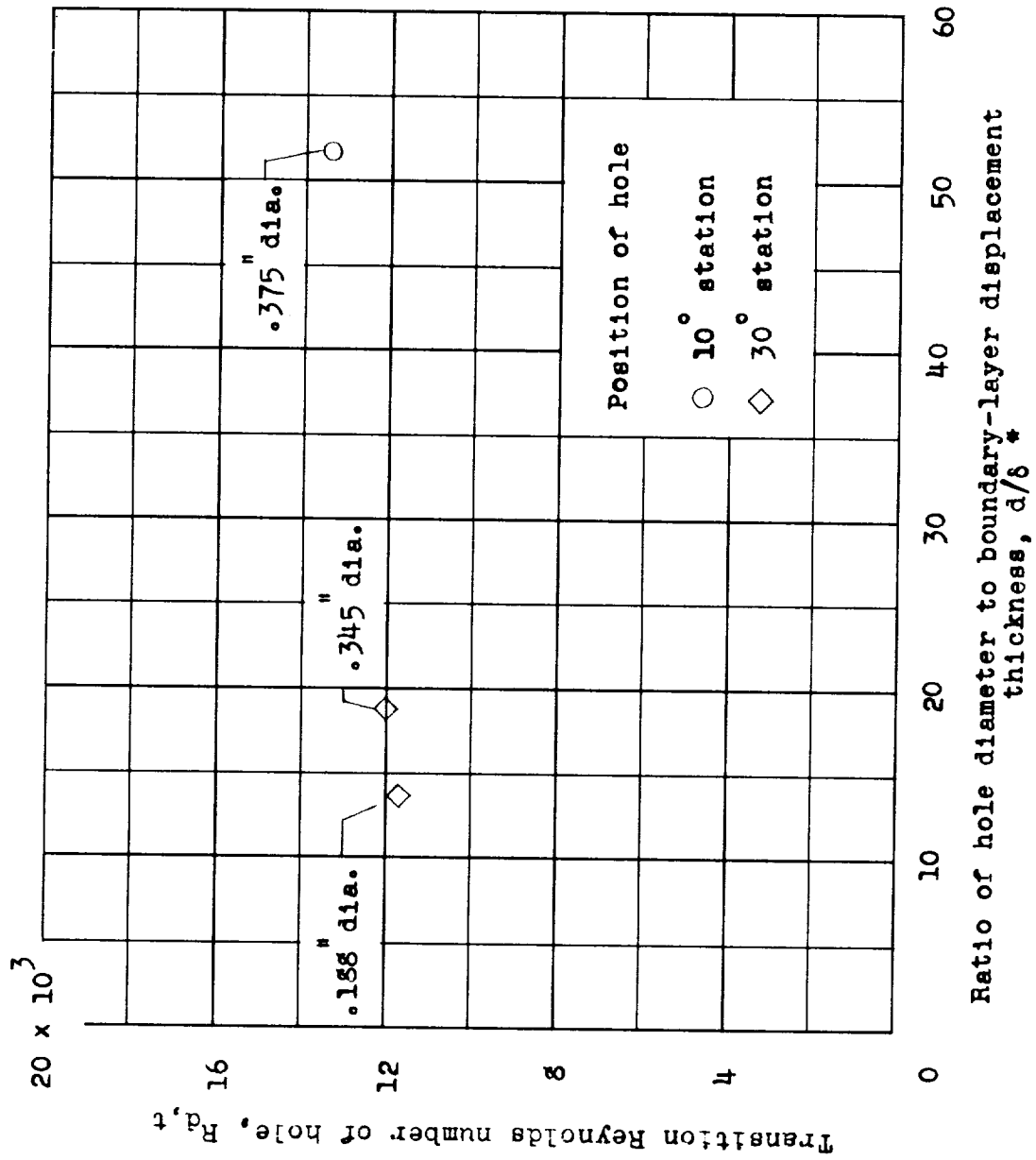


Figure 16.- Transition Reynolds number on hemisphere for holes with a large  $h/d$ .

<p>NASA MEMO 2-8-59L National Aeronautics and Space Administration. AN INVESTIGATION OF THE EFFECT OF A HIGHLY FAVORABLE PRESSURE GRADIENT ON BOUNDARY-LAYER TRANSITION AS CAUSED BY VARIOUS TYPES OF ROUGHNESSES ON A 10-FOOT- DIAMETER HEMISPHERE AT SUBSONIC SPEEDS. John B. Peterson, Jr., and Elmer A. Horton. April 1959. 32p. diagrs., photos., tabs. (NASA MEMORANDUM 2-8-59L)</p> <p>Tests were conducted at Reynolds numbers up to 10 x 10<sup>6</sup> and at a maximum Mach number of about 0.1 which show that the occurrence of transition behind three-dimensional particle types of roughness could be correlated with the roughness Reynolds num- ber. Results of tests with two-dimensional types of roughness are presented which show the effects of wire and scratch types of roughness on transition. Also included in the investigation were studies of the spread of turbulence behind a single roughness particle (over)</p> <p>Copies obtainable from NASA, Washington</p>	<ol style="list-style-type: none"><li>1. Flow, Laminar (1.1.3.1)</li><li>2. Flow, Turbulent (1.1.3.2)</li><li>3. Bodies - Surface Con- ditions (1.3.2.4)</li></ol> <ol style="list-style-type: none"><li>I. Peterson, John B., Jr.</li><li>II. Horton, Elmer A.</li><li>III. NASA MEMO 2-8-59L</li></ol> <p style="text-align: right;">NASA</p>	<p>NASA MEMO 2-8-59L National Aeronautics and Space Administration. AN INVESTIGATION OF THE EFFECT OF A HIGHLY FAVORABLE PRESSURE GRADIENT ON BOUNDARY-LAYER TRANSITION AS CAUSED BY VARIOUS TYPES OF ROUGHNESSES ON A 10-FOOT- DIAMETER HEMISPHERE AT SUBSONIC SPEEDS. John B. Peterson, Jr., and Elmer A. Horton. April 1959. 32p. diagrs., photos., tabs. (NASA MEMORANDUM 2-8-59L)</p> <p>Tests were conducted at Reynolds numbers up to 10 x 10<sup>6</sup> and at a maximum Mach number of about 0.1 which show that the occurrence of transition behind three-dimensional particle types of roughness could be correlated with the roughness Reynolds num- ber. Results of tests with two-dimensional types of roughness are presented which show the effects of wire and scratch types of roughness on transition. Also included in the investigation were studies of the spread of turbulence behind a single roughness particle (over)</p> <p>Copies obtainable from NASA, Washington</p>	<ol style="list-style-type: none"><li>1. Flow, Laminar (1.1.3.1)</li><li>2. Flow, Turbulent (1.1.3.2)</li><li>3. Bodies - Surface Con- ditions (1.3.2.4)</li></ol> <ol style="list-style-type: none"><li>I. Peterson, John B., Jr.</li><li>II. Horton, Elmer A.</li><li>III. NASA MEMO 2-8-59L</li></ol> <p style="text-align: right;">NASA</p>
<p>NASA MEMO 2-8-59L National Aeronautics and Space Administration. AN INVESTIGATION OF THE EFFECT OF A HIGHLY FAVORABLE PRESSURE GRADIENT ON BOUNDARY-LAYER TRANSITION AS CAUSED BY VARIOUS TYPES OF ROUGHNESSES ON A 10-FOOT- DIAMETER HEMISPHERE AT SUBSONIC SPEEDS. John B. Peterson, Jr., and Elmer A. Horton. April 1959. 32p. diagrs., photos., tabs. (NASA MEMORANDUM 2-8-59L)</p> <p>Tests were conducted at Reynolds numbers up to 10 x 10<sup>6</sup> and at a maximum Mach number of about 0.1 which show that the occurrence of transition behind three-dimensional particle types of roughness could be correlated with the roughness Reynolds num- ber. Results of tests with two-dimensional types of roughness are presented which show the effects of wire and scratch types of roughness on transition. Also included in the investigation were studies of the spread of turbulence behind a single roughness particle (over)</p> <p>Copies obtainable from NASA, Washington</p>	<ol style="list-style-type: none"><li>1. Flow, Laminar (1.1.3.1)</li><li>2. Flow, Turbulent (1.1.3.2)</li><li>3. Bodies - Surface Con- ditions (1.3.2.4)</li></ol> <ol style="list-style-type: none"><li>I. Peterson, John B., Jr.</li><li>II. Horton, Elmer A.</li><li>III. NASA MEMO 2-8-59L</li></ol> <p style="text-align: right;">NASA</p>	<p>NASA MEMO 2-8-59L National Aeronautics and Space Administration. AN INVESTIGATION OF THE EFFECT OF A HIGHLY FAVORABLE PRESSURE GRADIENT ON BOUNDARY-LAYER TRANSITION AS CAUSED BY VARIOUS TYPES OF ROUGHNESSES ON A 10-FOOT- DIAMETER HEMISPHERE AT SUBSONIC SPEEDS. John B. Peterson, Jr., and Elmer A. Horton. April 1959. 32p. diagrs., photos., tabs. (NASA MEMORANDUM 2-8-59L)</p> <p>Tests were conducted at Reynolds numbers up to 10 x 10<sup>6</sup> and at a maximum Mach number of about 0.1 which show that the occurrence of transition behind three-dimensional particle types of roughness could be correlated with the roughness Reynolds num- ber. Results of tests with two-dimensional types of roughness are presented which show the effects of wire and scratch types of roughness on transition. Also included in the investigation were studies of the spread of turbulence behind a single roughness particle (over)</p> <p>Copies obtainable from NASA, Washington</p>	<ol style="list-style-type: none"><li>1. Flow, Laminar (1.1.3.1)</li><li>2. Flow, Turbulent (1.1.3.2)</li><li>3. Bodies - Surface Con- ditions (1.3.2.4)</li></ol> <ol style="list-style-type: none"><li>I. Peterson, John B., Jr.</li><li>II. Horton, Elmer A.</li><li>III. NASA MEMO 2-8-59L</li></ol> <p style="text-align: right;">NASA</p>

NASA MEMO 2-8-59L

and the effects of holes such as pressure orifices on boundary-layer transition.

NASA MEMO 2-8-59L

and the effects of holes such as pressure orifices on boundary-layer transition.

Copies obtainable from NASA, Washington

NASA MEMO 2-8-59L

and the effects of holes such as pressure orifices on boundary-layer transition.

NASA

Copies obtainable from NASA, Washington

NASA MEMO 2-8-59L

and the effects of holes such as pressure orifices on boundary-layer transition.

NASA

Copies obtainable from NASA, Washington

NASA

Copies obtainable from NASA, Washington

NASA